



Hyperreflective foci in the choroid of normal eyes

Young Ho Kim¹ · Jaeryung Oh¹

Received: 11 May 2021 / Revised: 11 August 2021 / Accepted: 15 October 2021 / Published online: 21 October 2021
© The Author(s), under exclusive licence to Springer-Verlag GmbH Germany, part of Springer Nature 2021

Abstract

Purpose To investigate hyperreflective choroidal foci (HCF) using en face swept-source optical coherence tomography (SS-OCT) and determine the factors that contribute to the distribution of HCF in normal eyes.

Methods In this retrospective study, we included healthy eyes with a normal fundus. HCF were defined as hyperreflective spots on en face SS-OCT images. The number, mean area, total area, and circularity of the HCF were compared with various choroid measurements obtained using SS-OCT, SS-OCT angiography, and fundus photography.

Results We investigated 51 eyes from 51 patients. The mean patient age was 56.0 ± 14.7 years, and 32 (62.7%) were female. The number and total area of HCF did not differ between the female and male patients and the right and left eyes. The number of HCF was correlated with the stromal area of the choroid ($r = 0.291$, $P = 0.040$) and subfoveal choroidal vascularity index ($r = -0.364$, $P = 0.009$). The total area of HCF was correlated with the stromal area of the choroid ($r = 0.283$, $P = 0.045$). However, the number and total area of HCF were not correlated with age, degree of macular tessellation, subfoveal choroidal thickness, and choriocapillaris vascular density and flow void area.

Conclusion HCF were observed in normal eyes, and their distribution was associated with the underlying stromal component of the choroid. The results of this study can be used as a reference for determining abnormal hyperreflective foci in the choroid of the eyes with various diseases.

Key messages

- Hyperreflective foci (HCF) have been described in various retinal diseases.
- HCF were observed in normal eyes, and their distribution was associated with the underlying stromal component of the choroid.
- The number and total area of HCF were positively correlated with the stromal area of the choroid, whereas the number of HCF was negatively correlated with the subfoveal choroidal vascularity index.
- The distribution of HCF did not differ by age or sex.

Keywords Choriocapillaris · Choroid · Choroidal vascularity · Fundus tessellation · Hyperreflective foci · Swept-source optical coherence tomography

Introduction

Hyperreflective spots or foci are small, well-circumscribed punctiform lesions with higher reflectivity similar to that of nerve fibre layer and have a scattered distribution within all layers of the neurosensory retina, on optical coherence tomography (OCT) [1]. Hyperreflective foci have been demonstrated in various retinal diseases [2–11], including

✉ Jaeryung Oh
ojr4991@korea.ac.kr; ojr4991@yahoo.co.kr

¹ Department of Ophthalmology, Korea University College of Medicine, 73 Goryeodae-ro, Sungbuk-ku, Seoul, South Korea 02841

diabetic macular oedema, retinal vein occlusion, age-related macular degeneration, polypoidal choroidal vasculopathy, central serous chorioretinopathy, and retinitis pigmentosa. Vujosevic et al. [12] reported that hyperreflective spots were also present in the normal retina.

In addition to the retinal layers, hyperreflective foci have been observed in various locations, such as the vitreous, subretinal, and subretinal pigment epithelium spaces, with diverse distribution patterns according to different chorioretinal diseases [7, 13–16]. In the eyes with serous retinal detachment type of macular oedema caused by diabetic retinopathy or retinal vein occlusion, hyperreflective foci were found to be attached underneath the outer border of the detached neurosensory retina [7, 15, 16], while they were clustered around the leaking point, where confirmed using fluorescein angiography of the eyes with central serous chorioretinopathy [17]. Recently, several studies have demonstrated the presence of hyperreflective choroidal foci (HCF) [18–20].

The advancement of spectral-domain OCT (SD-OCT) technology has enabled acquisition of detailed retinal images for various diseases. Most studies have identified hyperreflective foci on the B-scan of SD-OCT [1–12, 15–18]. Only a few studies have investigated hyperreflective foci using en face OCT images [12, 21, 22]. In addition to the enhanced depth imaging technique, the introduction of swept-source OCT (SS-OCT) has allowed acquisition of detailed choroid images [23–25]. The choroidal thickness and choroidal vascularity can be measured in vivo using SS-OCT. However, the factors affecting distribution of HCF in the normal eye are not yet clear.

In this study, we hypothesized that choroidal structure may affect the presence and distribution of HCF in the normal choroid. We measured HCF quantitatively using en face SS-OCT and determined the factors contributing to the distribution of HCF in normal eyes.

Methods

This retrospective study was approved by the Institutional Review Board of Korea University Anam Hospital, and all research and data collection procedures were performed in accordance with the tenets of the Declaration of Helsinki. We searched the SS-OCT database of Korea University Anam Hospital between March 2016 and December 2020 and included patients with a normal fundus. We reviewed their medical history and included only healthy eyes. The patients underwent a complete ophthalmic examination, including best corrected visual acuity measurement, biomicroscopy, intraocular pressure assessment, fundus photography, SS-OCT, and SS-OCT angiography (SS-OCTA). We excluded the eyes with pigment epitheliopathy or drusen and

the eyes with high myopia (axial length ≥ 28.0 mm), diabetic retinopathy, retinal vascular diseases, a history of uveitis, central serous chorioretinopathy, ocular surgery except cataract surgery, and cataract surgery within 6 months before measurement. The eyes with poor quality SS-OCT and SS-OCTA images (image quality score in arbitrary units < 60) were excluded.

We acquired all SS-OCT and SS-OCTA images using DRI OCT Triton (Topcon Corp., Tokyo, Japan; software version 10.10), which operates at an A-scan speed of 100,000 per second and uses a central wavelength of 1050 nm. Under ideal scan conditions, this instrument had an axial resolution of 8 μm and a transverse resolution of 20 μm for examining tissues.

Selection of choroidal slab

A three-dimensional (3D) macular cube scan was acquired over a 3000×3000 - μm area centred on the fovea during the SS-OCTA default scanning protocol. Each B-scan was produced from 320 A-scans, and each cube scan composed 320 horizontal B-scans. A 3000×3000 - μm OCTA protocol had four repetitions of the B-scan at each position. The automated instrument's algorithm was used to segment all retinal layers and Bruch's membrane. For further imaging analysis, a 3000×3000 - μm en face structural SS-OCT image, consisting of 320×320 pixels, was generated from this macular cube scan using the built-in software. A single experienced retinal specialist (J.O.) assessed the segmentation error, and high-quality images without significant segmentation errors were used for further analysis. To reduce the projection artefact of overlying retinal vessels and the effect of underlying large choroidal vessels, we selected a choroidal layer slab between 5.2 and 20.8 μm below the Bruch's membrane. This choroidal layer slab improved the HCF visibility [26].

HCF on en face SS-OCT

HCF were defined as spots with reflectivity beyond two standard deviations (SDs) of the mean reflectivity in the selected slab (Fig. 1) on en face structural SS-OCT images. HCF were determined on a previously selected choroidal layer slab (Fig. 2). After the display setting of the colour of SS-OCT was set to reverse black/white, segmentation lines for the en face choriocapillaris layer image were moved to 5.2 μm and 20.8 μm below the Bruch's membrane to obtain the choroidal layer slab of the en face image for HCF measurement. The en face images were exported and analysed using ImageJ (<http://imagej.nih.gov/ij/>; provided in the public domain by the National Institutes of Health) software. After conversion of reversed images to 8-bit grayscale, the measurement scale was set from 320 pixel to 3000 μm . Thereafter, the image's histogram was analysed, and the

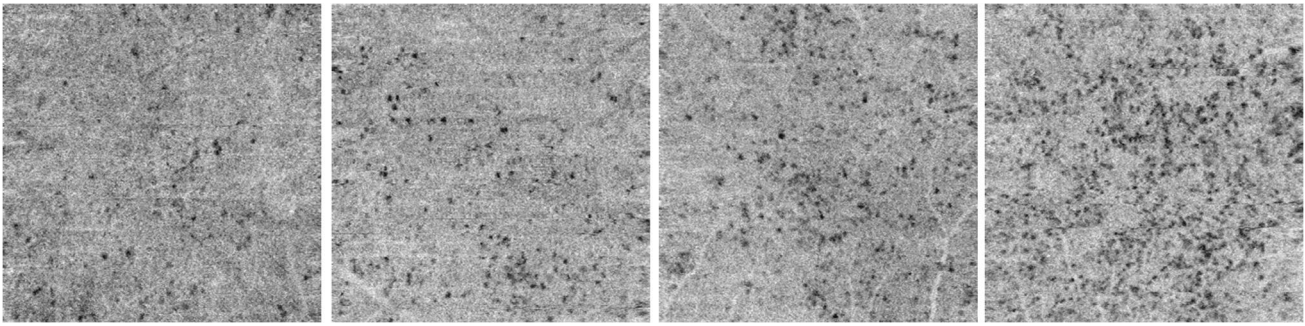


Fig. 1 En face swept-source optical coherence tomographic images of hyperreflective choroidal foci

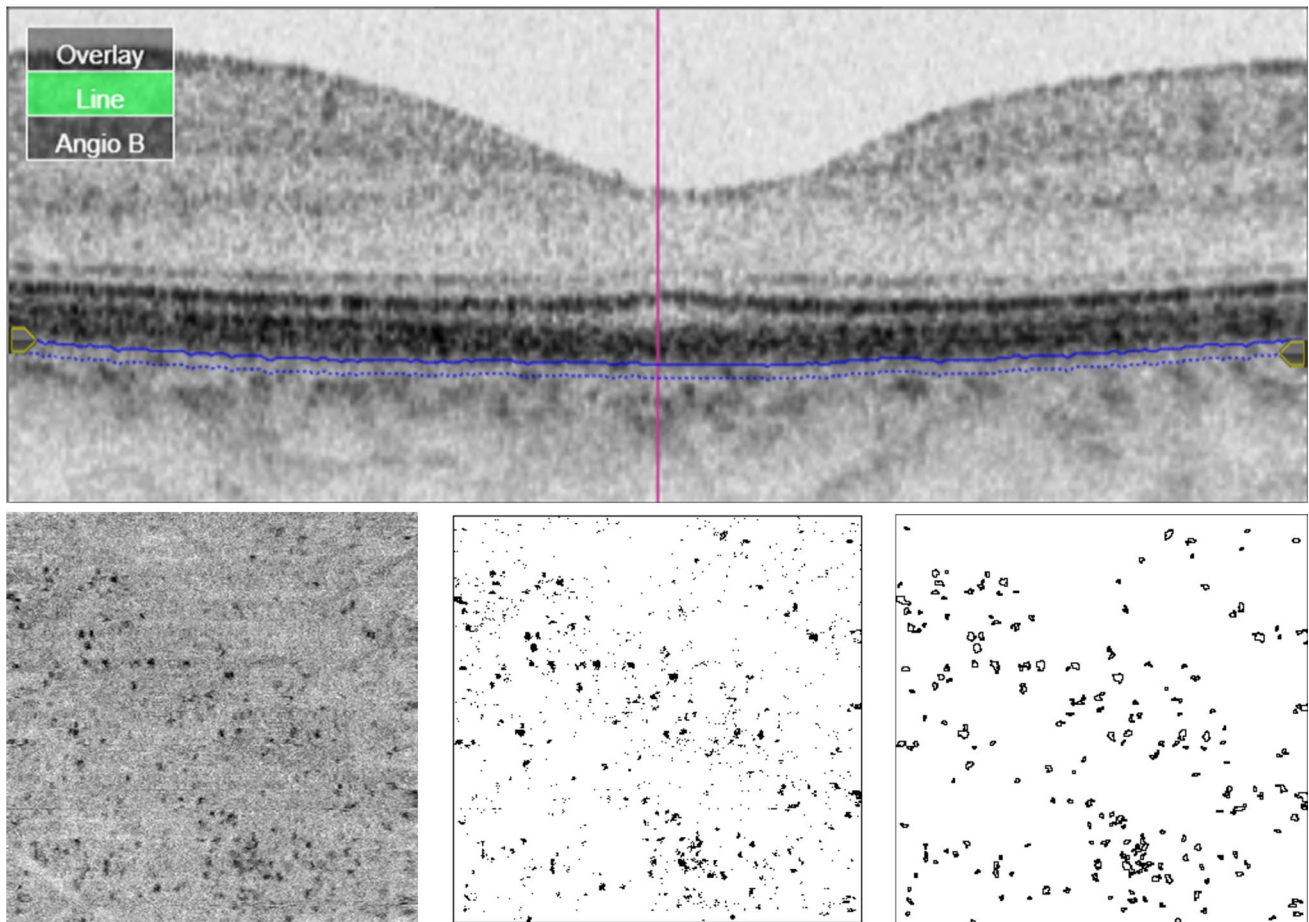


Fig. 2 The partial choroidal layer slab (lower left) including the data from a Bruch’s membrane-based 15.6- μm -thick slab positioned 5.2 μm under the Bruch’s membrane was obtained from en face SS-OCT images retrieved during SS-OCTA scanning performed in a 3000 \times 3000- μm area centred on the macula (upper). Hyperreflective choroidal foci were defined as spots with reflectivity beyond two

standard deviations of the mean reflectivity in the selected slab (lower middle). To prevent counting noise signal, we selected the particles with area $\geq 314 \mu\text{m}^2$ (lower right). SS-OCT, swept-source optical coherence tomography; SS-OCTA, swept-source optical coherence tomography angiography

reflectivity threshold level for the HCF was set at two SDs below the mean of the reflectivity from the histogram. The image was processed using a binarization tool with a

watershed function to separate overlapping spots. HCF were measured using an analysed particle tool to trace the boundary of the hyperreflective foci. To prevent counting noise

signal as HCF, we defined the minimum diameter and area of HCF as $20\ \mu\text{m}$ and $314\ \mu\text{m}^2$, respectively [18]. Any particle of area from $314\ \mu\text{m}^2$ to infinity on the ImageJ tool was noted. The number, total area, mean size, and circularity of HCF were calculated.

Choroidal thickness and choroidal vascularity index on SS-OCT

Subfoveal choroidal thickness was measured using SS-OCT images. SS-OCT images at the macula were obtained with a three-dimensional horizontal volume scan plus 5-line raster cross protocol, which was provided by the manufacturer. Among five horizontal and five vertical line scans, each averaged from 96 B-scan images, we measured the subfoveal choroidal thickness using a 9-mm horizontal line scan passing through the foveal centre. Subfoveal choroidal thickness was measured manually from the retinal pigment epithelium (RPE)/Bruch's membrane complex to the choroidoscleral interface at the centre of the fovea using the calliper tool of the instrument's image viewer programme, as previously reported [27, 28]. Two independent observers (Y.H.K. and J.O.) blinded to patient information independently measured subfoveal choroidal thickness, and the mean value was used for further statistical analysis.

Choroidal vascularity index (CVI) was defined as the ratio of the luminal area to the total choroidal area [29]. We measured CVI using the same 9-mm horizontal line scan image as used for the measurement of subfoveal choroidal

thickness using our previously reported method (Fig. 3) [28, 30].

Choriocapillaris flow on SS-OCTA

The vascular density (VD) and flow void area of the choriocapillaris layer were measured on SS-OCTA images as described previously [31]. In brief, the SS-OCTA images were obtained using a $3000 \times 3000\text{-}\mu\text{m}$ OCTA scan of the macula, and automated layer segmentation was obtained, as described above. The en face SS-OCTA image of the choriocapillaris was generated from the slab with a position between 0 and $10.4\ \mu\text{m}$ below the Bruch's membrane, which is a default setting provided by the instrument's software. The en face OCTA images were exported and analysed using ImageJ software. The detailed methods for the measurements of vascular density (VD) and flow void area of the choriocapillaris are described in Online Resource 1 and our previously published study [31].

Grading of macular tessellation in fundus photography

Colour fundus photography was obtained when SS-OCT scan was performed using the built-in fundus camera of the instrument. Macular tessellation on colour fundus photography was quantitatively evaluated using the macular tessellated fundus index (TFI) [32, 33]. To evaluate the corresponding area of the en face OCT images, we made some

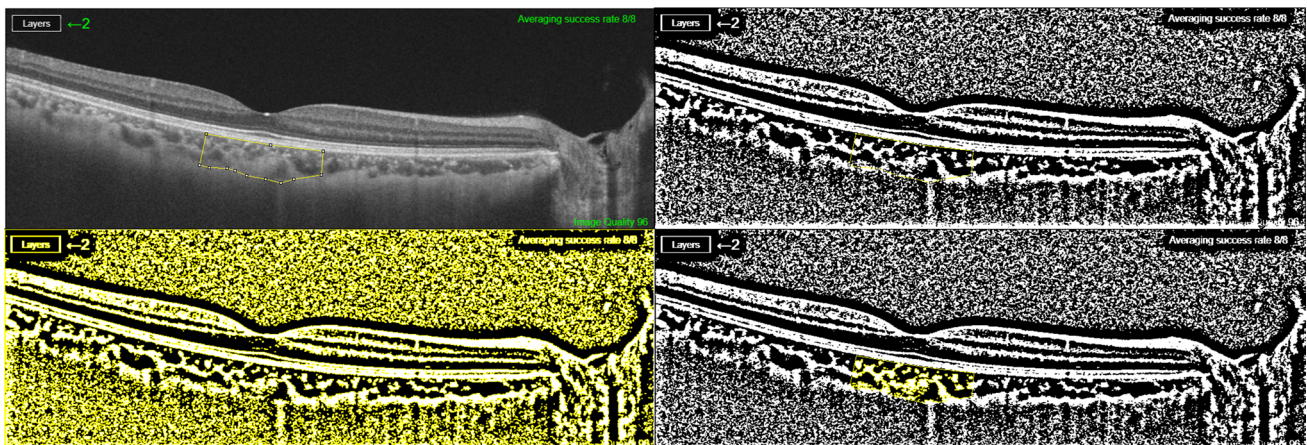


Fig. 3 Measurement of choroidal vascular index (CVI). CIV was measured on the 9-mm horizontal line scan passing through the fovea, which produced from the averaging of 96 B-scans. Using a polygon tool, the total choroidal area with a width of $1500\ \mu\text{m}$, centred on the fovea, was manually selected as the region of interest (ROI). The inner and outer boundaries of the total choroidal area were traced along the RPE/Bruch's membrane complex and the choroidoscleral junction, respectively. (upper left). After conversion to 8-bit grayscale, image binarization for demarcation of the choroidal vascular

and stromal areas was performed using an auto local thresholding tool with the Niblack method (upper right). The binarized image was converted back to a red, green, blue (RGB) image, and the colour threshold tool was applied to determine the dark pixel, which represent the luminal area (lower left), and the luminal area was determined using merged images with initially selected the region of interest (lower right). Thereafter, the stromal area was calculated by subtracting the luminal area from the total choroidal area, and CVI was calculated by dividing the luminal area by the total choroidal area

modifications to the previously proposed method for selecting the ROI. While carefully observing the vascular shape of the macula, we selected a $3000 \times 3000\text{-}\mu\text{m}$ rectangular area centred on the fovea as the ROI (Fig. 4). Thereafter, the colour fundus photographs were split into red, green, and blue pixels using the RGB stack tool. A histogram was constructed for each colour, and the mean intensities of red (R), green (G), and blue (B) pixels within the rectangular area were determined. As previously proposed by Yoshihara et al. [33], we also calculated three variations in TFIs, namely TFI-1, TFI-2, and TFI-3. The three TFIs were determined according to the following equations: $\text{TFI-1} = (\text{R}-\text{G})/\text{R}$, $\text{TFI-2} = \text{R}/(\text{R} + \text{G} + \text{B})$, and $\text{TFI-3} = (\text{R}-\text{G})/(\text{R} + \text{G} + \text{B})$.

Statistical analysis

All statistical analyses were performed using IBM SPSS Statistics for Windows, version 20.0 (IBM Corp., Armonk, NY, USA). The baseline characteristics were compared using a Student's *t*-test for continuous variables and χ^2 test

for categorical variables. Pearson's correlation coefficient (*r*) was used to analyse the linear correlations of various variables with HCF. Statistical significance was set at $P < 0.05$.

Results

General characteristics

We investigated 51 eyes from 51 normal subjects (Table 1). The mean patient age was 56.0 ± 14.7 years, and 32 (62.7%) were female. The number and total area of HCF did not differ between the female and male patients and the right and left eyes (Table 2).

Correlation of HCF with various parameters

The mean number of HCF was 224.6 ± 44.8 in a $3000 \times 3000\text{-}\mu\text{m}$ area. The mean size of HCF was $937.3 \pm 119.8 \mu\text{m}^2$. The mean number and total area of HCF did not correlate

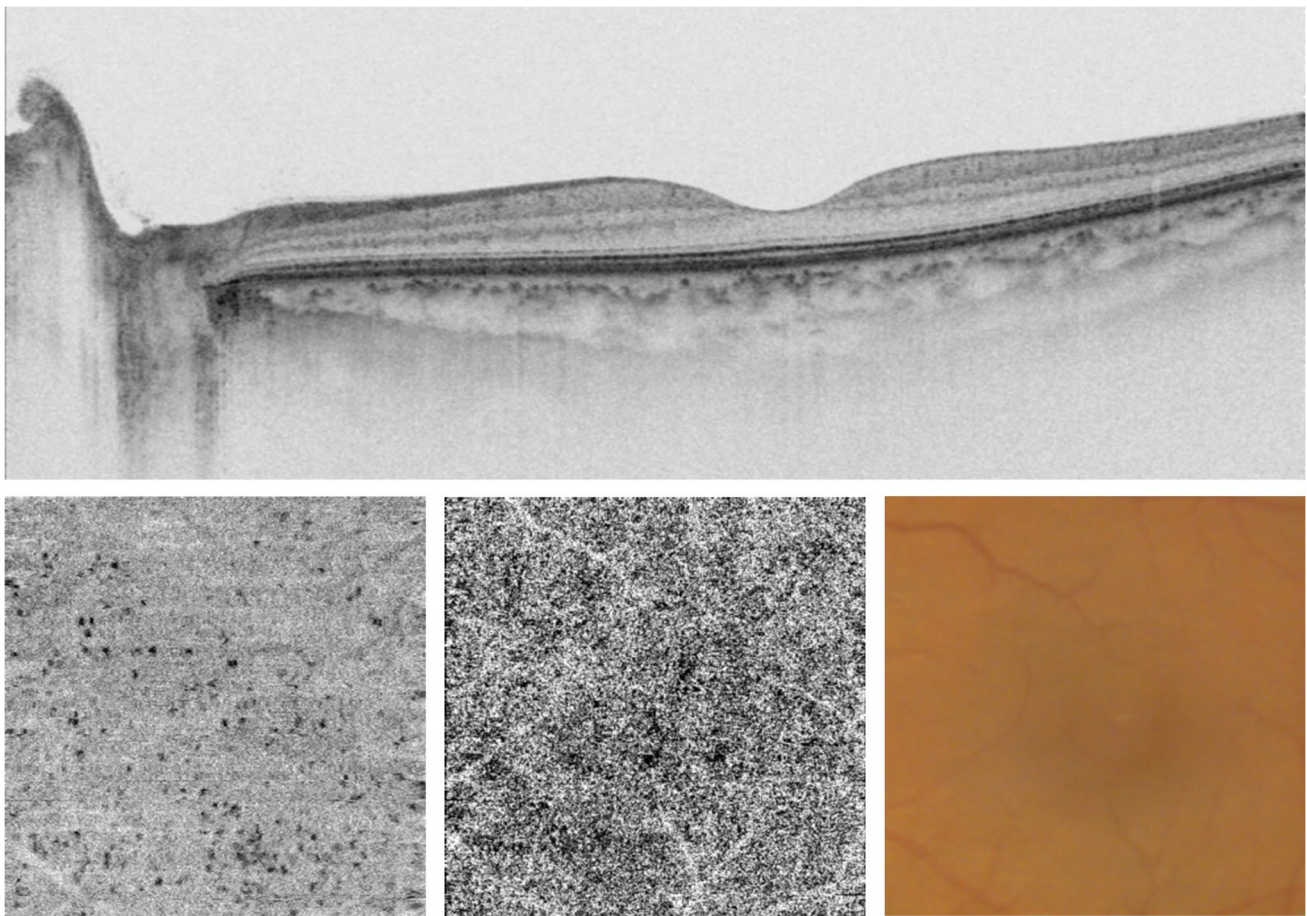


Fig. 4 Hyperreflective choroidal foci on the B-scan image of swept-source optical coherence tomography (SS-OCT) (upper) and en face images of SS-OCT covering the rectangular area of $3000 \times 3000\text{-}\mu\text{m}$, centred on the macula (lower left), choriocapillaris layer images obtained using SS-OCT angiography (lower centre), colour fundus photography images (lower right)

μm , centred on the macula (lower left), choriocapillaris layer images obtained using SS-OCT angiography (lower centre), colour fundus photography images (lower right)

Table 1 Characteristics of the subjects

Variables	Mean \pm SD
Number of eyes	51
Age, years	56.0 \pm 14.7
Sex, n (%)	
Female: male	32 (62.7%): 19 (37.3%)
Eye, n (%)	
Right: left	24 (47.1%): 27 (52.9%)
Diabetes, n (%)	14 (27.5%)
Hypertension, n (%)	7 (13.7%)
HCF	
Number	224.6 \pm 44.8
Total area, μm^2	211,974 \pm 54,095
Mean size, μm^2	937.3 \pm 119.8
Circularity	0.65 \pm 0.03
Choroid	
Subfoveal choroidal thickness, μm	283.1 \pm 87.2
Choroidal vascularity index, %	61.88 \pm 5.51
Choroidal area, μm^2	455,986 \pm 94,792
Luminal area, μm^2	284,092 \pm 70,097
Stromal area, μm^2	171,894 \pm 35,450
Choriocapillaris	
Vascular density	136.4 \pm 3.4
Flow void area, μm^2	527,077 \pm 275,900
Degree of tessellation	
TFI-1	0.442 \pm 0.045
TFI-2	0.557 \pm 0.026
TFI-3	0.247 \pm 0.036

SD standard deviation, HCF hyperreflective choroidal foci, TFI tessellated fundus index

with age, subfoveal choroidal thickness, choriocapillaris VD and flow void area, and the degree of macular tessellation (Table 3). However, the mean number of HCF correlated with the subfoveal CVI ($r = -0.363$, $P = 0.009$) and stromal area of the choroid ($r = 0.283$, $P = 0.045$). The total area of HCF was also correlated with the stromal area of the choroid ($r = 0.283$, $P = 0.045$). The circularity of HCF correlated with age ($r = -0.330$, $P = 0.018$) and choriocapillaris VD ($r = 0.335$, $P = 0.016$).

Partial correlation coefficient while controlling for the difference in image quality Several factors of HCF, such as number and circularity, tended to vary with OCT image quality, even though only high-quality OCT images were included in this study (Table 4). For this confounding factor, we analysed the partial correlation while controlling for differences in the quality of the OCT images (Table 5). We found that the number of HCF was still correlated with the subfoveal CVI ($r = -0.364$, $P = 0.009$) and stromal area of the choroid ($r = 0.291$, $P = 0.040$) (Fig. 5). However, the correlation between the circularity of HCF and other parameters was not significant.

Discussion

Hyperreflective foci have been studied in the eyes with chorioretinal diseases. They were believed to be activated microglial cells in several previous studies [2, 11, 18, 34]. Roy et al. [19] suggested that hyperreflective foci within the choroid have a composition similar to that of hyperreflective foci within the retina of the eyes with diabetic macular oedema. Romano et al. [20] hypothesized that macrophage recruitment or progressive RPE degeneration may

Table 2 Comparison of the parameters of HCF in relation to sex, side of the eyes, and systemic factors

Variables	Number of HCF		Total area of HCF, μm^2		Mean size of HCF, μm^2		Circularity of HCF	
	Mean (SD)	<i>P</i> value	Mean (SD)	<i>P</i> value	Mean (SD)	<i>P</i> value	Mean (SD)	<i>P</i> value
Sex								
Female	220.9 (40.7)	0.446	207,106.0 (56,232.1)	0.410	926.4 (128.8)	0.403	0.651 (0.028)	0.616
Male	230.9 (51.5)		220,175.3 (50,692.7)		955.8 (103.7)		0.647 (0.034)	
Eye								
Right	229.8 (52.8)	0.452	223,073.7 (64,650.9)	0.182	958.0 (124.8)	0.250	0.647 (0.029)	0.617
Left	220.0 (36.8)		202,109.4 (41,415.9)		919.0 (114.4)		0.652 (0.031)	
Diabetes								
Yes	234.4 (37.9)	0.341	223,700.5 (46,749.6)	0.346	951.4 (110.8)	0.611	0.647 (0.030)	0.650
No	220.9 (47.1)		207,538.3 (56,581.0)		932.0 (124.1)		0.651 (0.030)	
Hypertension								
Yes	227.6 (24.2)	0.853	217,366.1 (42,895.0)	0.780	959.8 (198.8)	0.745	0.656 (0.040)	0.531
No	224.1 (47.5)		211,117.3 (56,039.8)		933.8 (105.3)		0.649 (0.029)	

HCF hyperreflective choroidal foci, SD standard deviation

P values are estimated by independent t test

Table 3 Correlation between number and area of hyperreflective choroidal foci and other parameters

Variables	Number of HCF		Total area of HCF		Mean size of HCF		Circularity of HCF	
	<i>r</i>	<i>P</i> value	<i>r</i>	<i>P</i> value	<i>r</i>	<i>P</i> value	<i>r</i>	<i>P</i> value
Age, years	0.081	0.572	0.092	0.523	0.046	0.746	-0.330	0.018*
Choroid								
Subfoveal choroidal thickness, μm	-0.084	0.560	-0.006	0.964	0.127	0.374	0.135	0.343
Choroidal vascularity index, %	-0.363	0.009*	-0.258	0.068	0.024	0.868	0.056	0.699
Choroidal area, μm ²	0.043	0.766	0.142	0.319	0.243	0.086	-0.133	0.352
Luminal area, μm ²	-0.074	0.606	0.049	0.730	0.227	0.109	-0.094	0.513
Stromal area, μm ²	0.260	0.065	0.283	0.045*	0.201	0.157	-0.170	0.233
Choriocapillaris layer								
Vascular density	-0.045	0.753	-0.074	0.606	-0.043	0.763	0.335	0.016*
Flow void area, μm ²	0.062	0.665	0.069	0.632	0.006	0.968	-0.236	0.095
Degree of macular tessellation								
TFI 1	-0.173	0.226	-0.190	0.183	-0.146	0.308	0.022	0.876
TFI 2	-0.169	0.236	-0.189	0.184	-0.158	0.267	0.037	0.797
TFI 3	-0.168	0.238	-0.188	0.185	-0.152	0.287	0.027	0.849

HCF hyperreflective choroidal foci, SD standard deviation, TFI tessellated fundus index

**P* value < 0.05 by Pearson's correlation

Table 4 Correlation between the quality of the optical coherence tomographic images and measurements of HCF

HCF measurements	<i>r</i>	<i>P</i> value
Number	0.251	0.075
Total area	0.176	0.216
Mean size	-0.055	0.700
Circularity	0.458	0.001*

HCF hyperreflective choroidal foci

**P* value < 0.05 by Pearson's correlation

be associated with the origin of hyperreflective foci in the eyes with choroideremia. Piri et al. [18] suggested that the predominant distribution of hyperreflective foci in the choroid and inner retina in Stargardt disease results from the spreading of lipofuscin deposits, which are by-products of the outer segment of the photoreceptor in the outer retina. However, they acknowledged several limitations present in concluding the origin, nature, and significance of HCF. In our study, we showed that hyperreflective foci exist in the choroid of normal eyes. Until now, it was not clear why hyperreflective foci were found in the normal choroid; our results may suggest an alternative possibility of their origin, which is different from inflammation or lipofuscin deposits.

In this study, we measured the number and area of HCF in the macular area between the choriocapillaris and Sattler's layers of the choroid. We compared the distribution of HCF with choroidal parameters assessed on SS-OCT and SS-OCTA and found that the number and area of HCF were correlated with the proportion of the stromal area of the

Table 5 Correlation between the number and circularity of HCF and other measurements while controlling for the quality of the optical coherence tomographic images

Variables	Number of HCF		Circularity of HCF	
	<i>r</i>	<i>P</i> value	<i>r</i>	<i>P</i> value
Age, years	0.157	0.275	-0.244	0.087
Choroid				
Subfoveal choroidal thickness, μm	-0.097	0.504	0.132	0.360
Choroidal vascularity index, %	-0.364	0.009*	0.084	0.564
Choroidal area, μm ²	0.063	0.665	-0.113	0.433
Luminal area, μm ²	-0.062	0.668	-0.077	0.595
Stromal area, μm ²	0.291	0.040*	-0.150	0.297
Choriocapillaris layer				
Vascular density	-0.134	0.354	0.228	0.111
Flow void area, μm ²	0.158	0.274	-0.103	0.476
Degree of macular tessellation				
TFI-1	-0.138	0.338	0.109	0.450
TFI-2	-0.145	0.314	0.102	0.481
TFI-3	-0.137	0.343	0.108	0.457

HCF hyperreflective choroidal foci, TFI tessellated fundus index

P values are estimated by partial while controlling for the difference in the quality of the OCT images

**P* value < 0.05

underlying choroid. The mean number of HCF was negatively correlated with the CVI. However, these parameters did not correlate with the vascularity of the choriocapillaris.

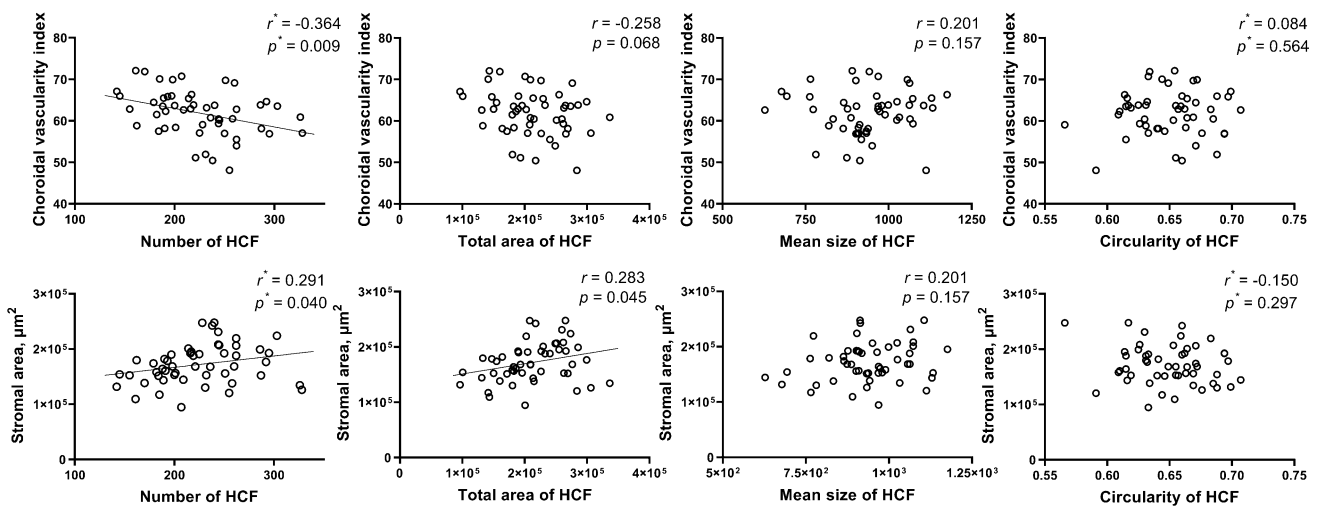


Fig. 5 Scattergram for the correlation of hyperreflective choroidal foci with various parameters. HCF, hyperreflective choroidal foci; r , Pearson's correlation; r^* , Partial correlation

These findings suggest that the distribution of HCF is related to the stroma of the choroid.

The choroid comprises both the stroma and vessels [35]. The choroidal stroma occupies the space between the dense vascular plexus and is composed of collagen and elastic fibres and several types of cells [35–37]. HCF may originate from some of these stromal components. In a previous human postmortem study, macrophages in the normal choroidal stroma were detected on using whole mounts of the choroid [38]. It suggests that HCF may be related to macrophages residing in normal choroid. In addition to macrophages, other candidates for the origin of HCF could be choroidal melanocytes [39–44]. Melanocytes have been reported to have high reflectivity on OCT images [45, 46]. Choroidal melanocytes are fusiform and dendritic cells that contain numerous round-to-ovoid discrete melanosomes [35–37]. Previous studies [35–37] have reported that the size of melanocyte in the choroid is larger than that in the skin, and the average length of choroidal melanocytes is approximately 20–40 μm with a diameter of approximately 20 μm . In our study, the mean size of HCF was $937.3 \pm 119.8 \mu\text{m}^2$, and the diameter was estimated to be 35.5 μm . These findings suggest that HCF could be of choroidal melanocytic origin. To compare the distribution of HCF with the colour of the fundus, we measured the TFI in the macular area. However, we could not find a significant correlation between the TFI and HCF. The measurement of the TFI at the macular centre, where the retina is rich in macular pigment, could have prevented a direct correlation between choroidal pigmentation and TFI. Further studies with images of the extra-macular area are required. Another candidate for the origin of HCF could be fibroblasts dispersed throughout the choroidal stroma. However, fibroblasts are not round

cells but spindle-shaped cells that often lie close to the choriocapillaris layer [47]. Further studies comparing OCT and the histology of normal eyes are needed to confirm the origin of HCF in the normal choroid.

Hyperreflective foci cannot be detected on clinical examination and have been variously defined using SD-OCT scans [10, 20]. In the current study using en face OCT images, we presented a method for quantitatively measuring HCF. B-scan images are useful for determining the relative location of hyperreflective foci in the chorioretinal layers. However, it is challenging to quantify the two-dimensional distribution of the foci in the coronal plane of the chorioretinal layers. We measured the distribution of hyperreflective foci on en face images of the choroid. It may help understand the two-dimensional distribution of foci and their relationship with fundus images. In addition, we defined hyperreflective foci based on the mean reflectivity of each en face image. This method would provide an objective quantification that is less dependent on the observers.

This study has some limitations, including its small sample size. The SS-OCT resolution of about 20 μm and the lack of histologic evidence prevented further detailed analysis of the relationship between the distribution of hyperreflective spots and specific choroidal constituents. Furthermore, we used only one type of SS-OCT and determined HCF in a slab near the choriocapillaris layer. This may have prevented further analysis of the correlation between the distribution of HCF and other parameters, such as choroidal thickness. Although we included high-quality images and statistically controlled the effect of image quality, signal noise was inevitable.

In conclusion, we found that the distribution of hyperreflective foci was associated with the underlying stromal

component of the choroid in normal eyes. The results of this study can help evaluate the origin of hyperreflective foci in the normal choroid and can be used as a reference in determining abnormal hyperreflective foci in the choroid of the eyes with various diseases.

Supplementary Information The online version contains supplementary material available at <https://doi.org/10.1007/s00417-021-05469-6>.

Author contribution Y.H.K.: data collection, imaging analysis, drafting the work, manuscript review, and final approval. J.O.: conception of the study, data collection, imaging analysis, interpretation of data, drafting of the work, manuscript review, and final approval. All authors read and approved the final manuscript.

Funding This work was supported by the Korea Medical Device Development Fund grant funded by the Korean government (Ministry of Science and ICT, Ministry of Trade, Industry and Energy, Ministry of Health & Welfare, Ministry of Food and Drug Safety) (Project Number: 1711137942, KMDF_PR_20200901_0026).

Availability of data and material We had full access to all the data in the study and take responsibility for the integrity of the data, the accuracy of the data analysis, and decision to submit for publication. The datasets generated and/or analysed during the current study are available from the corresponding author upon reasonable request.

Code availability Not applicable.

Declarations

Ethics approval This study was performed in accordance with the principles of the Declaration of Helsinki and approved by the Institutional Review Board of Korea University Anam Hospital, Seoul, Korea (IRB number: 2020AN0445).

Consent to participate This retrospective study involved no more than minimal risk to subjects, and the IRB of Korea University Anam Hospital approved our request to waive off the requirement of informed consent.

Consent for publication Not applicable.

Conflict of interest The authors declare no competing interests.

References

- Bolz M, Schmidt-Erfurth U, Deak G, Mylonas G, Kriechbaum K, Scholda C, Diabetic Retinopathy Research Group V (2009) Optical coherence tomographic hyperreflective foci: a morphologic sign of lipid extravasation in diabetic macular edema. *Ophthalmology* 116:914–920. <https://doi.org/10.1016/j.ophtha.2008.12.039>
- Vujosevic S, Bini S, Midena G, Berton M, Pilotto E, Midena E (2013) Hyperreflective intraretinal spots in diabetics without and with nonproliferative diabetic retinopathy: an in vivo study using spectral domain OCT. *J Diabetes Res* 2013:491835. <https://doi.org/10.1155/2013/491835>
- Framme C, Wolf S, Wolf-Schnurrbusch U (2010) Small dense particles in the retina observable by spectral-domain optical coherence tomography in age-related macular degeneration. *Invest Ophthalmol Vis Sci* 51:5965–5969. <https://doi.org/10.1167/iovs.10-5779>
- Coscas G, De Benedetto U, Coscas F, Li Calzi CI, Vismara S, Roudot-Thoraval F, Bandello F, Souied E (2013) Hyperreflective dots: a new spectral-domain optical coherence tomography entity for follow-up and prognosis in exudative age-related macular degeneration. *Ophthalmologica* 229:32–37. <https://doi.org/10.1159/000342159>
- Balaratnasingam C, Messinger JD, Sloan KR, Yannuzzi LA, Freund KB, Curcio CA (2017) Histologic and optical coherence tomographic correlates in drusenoid pigment epithelium detachment in age-related macular degeneration. *Ophthalmology* 124:644–656. <https://doi.org/10.1016/j.ophtha.2016.12.034>
- Lee H, Ji B, Chung H, Kim HC (2016) Correlation between optical coherence tomographic hyperreflective foci and visual outcomes after anti-vegf treatment in neovascular age-related macular degeneration and polypoidal choroidal vasculopathy. *Retina* 36:465–475. <https://doi.org/10.1097/IAE.0000000000000645>
- Ogino K, Murakami T, Tsujikawa A, Miyamoto K, Sakamoto A, Ota M, Yoshimura N (2012) Characteristics of optical coherence tomographic hyperreflective foci in retinal vein occlusion. *Retina* 32:77–85. <https://doi.org/10.1097/IAE.0b013e318217ffc7>
- Kang JW, Lee H, Chung H, Kim HC (2014) Correlation between optical coherence tomographic hyperreflective foci and visual outcomes after intravitreal bevacizumab for macular edema in branch retinal vein occlusion. *Graefes Arch Clin Exp Ophthalmol* 252:1413–1421. <https://doi.org/10.1007/s00417-014-2595-5>
- Maruko I, Iida T, Ojima A, Sekiryu T (2011) Subretinal dot-like precipitates and yellow material in central serous chorioretinopathy. *Retina* 31:759–765. <https://doi.org/10.1097/IAE.0b013e3181fbce8e>
- Lee H, Lee J, Chung H, Kim HC (2016) Baseline spectral domain optical coherence tomographic hyperreflective foci as a predictor of visual outcome and recurrence for central serous chorioretinopathy. *Retina* 36:1372–1380. <https://doi.org/10.1097/IAE.0000000000000929>
- Kuroda M, Hirami Y, Hata M, Mandai M, Takahashi M, Kurimoto Y (2014) Intraretinal hyperreflective foci on spectral-domain optical coherence tomographic images of patients with retinitis pigmentosa. *Clin Ophthalmol* 8:435–440. <https://doi.org/10.2147/OPHTH.S58164>
- Vujosevic S, Bini S, Torresin T, Berton M, Midena G, Parrozzani R, Martini F, Pucci P, Daniele AR, Cavarzeran F, Midena E (2017) Hyperreflective retinal spots in normal and diabetic eyes: B-scan and en face spectral domain optical coherence tomography evaluation. *Retina* 37:1092–1103. <https://doi.org/10.1097/IAE.0000000000001304>
- Saito M, Barbazetto IA, Spaide RF (2013) Intravitreal cellular infiltrate imaged as punctate spots by spectral-domain optical coherence tomography in eyes with posterior segment inflammatory disease. *Retina* 33:559–565. <https://doi.org/10.1097/IAE.0b013e31826710ea>
- Oh JH, Oh J, Roh HC (2017) Vitreous hyper-reflective dots in optical coherence tomography and retinal tear in patients with acute posterior vitreous detachment. *Curr Eye Res* 42:1179–1184. <https://doi.org/10.1080/02713683.2017.1289226>
- Ota M, Nishijima K, Sakamoto A, Murakami T, Takayama K, Horii T, Yoshimura N (2010) Optical coherence tomographic evaluation of foveal hard exudates in patients with diabetic maculopathy accompanying macular detachment. *Ophthalmology* 117:1996–2002. <https://doi.org/10.1016/j.ophtha.2010.06.019>
- Ajay K, Mason F, Gonglore B, Bhatnagar A (2016) Pearl necklace sign in diabetic macular edema: evaluation and significance. *Indian J Ophthalmol* 64:829–834. <https://doi.org/10.4103/0301-4738.195597>

17. Shinjima A, Hirose T, Mori R, Kawamura A, Yuzawa M (2010) Morphologic findings in acute central serous chorioretinopathy using spectral domain-optical coherence tomography with simultaneous angiography. *Retina* 30:193–202. <https://doi.org/10.1097/IAE.0b013e3181c70203>
18. Piri N, Nesmith BL, Schaal S (2015) Choroidal hyperreflective foci in Stargardt disease shown by spectral-domain optical coherence tomography imaging: correlation with disease severity. *JAMA Ophthalmol* 133:398–405. <https://doi.org/10.1001/jamaophthalmol.2014.5604>
19. Roy R, Saurabh K, Shah D, Chowdhury M, Goel S (2019) Choroidal hyperreflective foci: a novel spectral domain optical coherence tomography biomarker in eyes with diabetic macular edema. *Asia Pac J Ophthalmol (Phila)* 8:314–318. <https://doi.org/10.1097/APO.0000000000000249>
20. Romano F, Arrigo A, MacLaren RE, Charbel Issa P, Birtel J, Bandello F, Battaglia Parodi M (2020) Hyperreflective foci as a pathogenetic biomarker in choroideremia. *Retina* 40:1634–1640. <https://doi.org/10.1097/IAE.0000000000002645>
21. Nassisi M, Fan W, Shi Y, Lei J, Borrelli E, Ip M, Sadda SR (2018) Quantity of intraretinal hyperreflective foci in patients with intermediate age-related macular degeneration correlates with 1-year progression. *Invest Ophthalmol Vis Sci* 59:3431–3439. <https://doi.org/10.1167/iovs.18-24143>
22. Frizziero L, Parrozzani R, Midena G, Miglionico G, Vujosevic S, Pilotto E, Midena E (2016) Hyperreflective intraretinal spots in radiation macular edema on spectral domain optical coherence tomography. *Retina* 36:1664–1669. <https://doi.org/10.1097/iae.0000000000000986>
23. Ferrara D, Waheed NK, Duker JS (2016) Investigating the choriocapillaris and choroidal vasculature with new optical coherence tomography technologies. *Prog Retin Eye Res* 52:130–155. <https://doi.org/10.1016/j.preteyeres.2015.10.002>
24. Miller AR, Roisman L, Zhang Q, Zheng F, de Oliveira R, Dias J, Yehoshua Z, Schaal KB, Feuer W, Gregori G, Chu Z, Chen CL, Kubach S, An L, Stetson PF, Durbin MK, Wang RK, Rosenfeld PJ (2017) Comparison between spectral-domain and swept-source optical coherence tomography angiographic imaging of choroidal neovascularization. *Invest Ophthalmol Vis Sci* 58:1499–1505. <https://doi.org/10.1167/iovs.16-20969>
25. Zhou H, Chu Z, Zhang Q, Dai Y, Gregori G, Rosenfeld PJ, Wang RK (2018) Attenuation correction assisted automatic segmentation for assessing choroidal thickness and vasculature with swept-source OCT. *Biomed Opt Express* 9:6067–6080. <https://doi.org/10.1364/BOE.9.006067>
26. Zhang Q, Zheng F, Motulsky EH, Gregori G, Chu Z, Chen CL, Li C, de Sisternes L, Durbin M, Rosenfeld PJ, Wang RK (2018) A novel strategy for quantifying choriocapillaris flow voids using swept-source OCT angiography. *Invest Ophthalmol Vis Sci* 59:203–211. <https://doi.org/10.1167/iovs.17-22953>
27. Kim YH, Lee B, Kang E, Oh J (2021) Choroidal thickness profile and clinical outcomes in eyes with polypoidal choroidal vasculopathy. *Graefes Arch Clin Exp Ophthalmol* 259:1711–1721. <https://doi.org/10.1007/s00417-020-05051-6>
28. Lee B, Ahn J, Yun C, Kim SW, Oh J (2018) Variation of retinal and choroidal vasculatures in patients with age-related macular degeneration. *Invest Ophthalmol Vis Sci* 59:5246–5255. <https://doi.org/10.1167/iovs.17-23600>
29. Agrawal R, Salman M, Tan KA, Karampelas M, Sim DA, Keane PA, Pavesio C (2016) Choroidal vascularity index (CVI)-A novel optical coherence tomography parameter for monitoring patients with panuveitis? *PLoS ONE* 11:e0146344. <https://doi.org/10.1371/journal.pone.0146344>
30. Kim YH, Lee B, Kang E, Oh J (2021) Peripapillary choroidal vascularity outside the macula in patients with central serous chorioretinopathy. *Transl Vis Sci Technol* 10:9. <https://doi.org/10.1167/tvst.10.8.9>
31. Yun C, Nam KT, Park S, Hwang SY, Oh J (2020) Features of the choriocapillaris on four different optical coherence tomography angiography devices. *Int Ophthalmol* 40:325–333. <https://doi.org/10.1007/s10792-019-01182-w>
32. Neelam K, Chew RY, Kwan MH, Yip CC, Au Eong KG (2012) Quantitative analysis of myopic chorioretinal degeneration using a novel computer software program. *Int Ophthalmol* 32:203–209. <https://doi.org/10.1007/s10792-012-9542-4>
33. Yoshihara N, Yamashita T, Ohno-Matsui K, Sakamoto T (2014) Objective analyses of tessellated fundi and significant correlation between degree of tessellation and choroidal thickness in healthy eyes. *PLoS ONE* 9:e103586. <https://doi.org/10.1371/journal.pone.0103586>
34. Coscas G, Coscas F, Vismara S, Souied E, Soubrane G (2008) Spectral domain OCT in age-related macular degeneration: preliminary results with Spectralis HRA-OCT. *J Fr Ophtalmol* 31:353–361. [https://doi.org/10.1016/s0181-5512\(08\)71429-3](https://doi.org/10.1016/s0181-5512(08)71429-3)
35. Nickla DL, Wallman J (2010) The multifunctional choroid. *Prog Retin Eye Res* 29:144–168. <https://doi.org/10.1016/j.preteyeres.2009.12.002>
36. Nag TC, Kumari C (2017) Electron microscopy of the human choroid. In: Chhablani J, Ruiz-Medrano J (eds) *Choroidal Disorders*, 1st edn. Academic Press an imprint of Elsevier, London, pp 7–20
37. Heindl LM, Platzl C, Wolfmeier H, Herwig-Carl MC, Kaser-Eichberger A, Strohmaier C, Schroedl F (2021) Choroidal melanocytes: subpopulations of different origin? *Ann Anat* 238:151775. <https://doi.org/10.1016/j.aanat.2021.151775>
38. McLeod DS, Bhutto I, Edwards MM, Silver RE, Seddon JM, Luty GA (2016) Distribution and quantification of choroidal macrophages in human eyes with age-related macular degeneration. *Invest Ophthalmol Vis Sci* 57:5843–5855. <https://doi.org/10.1167/iovs.16-20049>
39. Delori FC, Pflibsen KP (1989) Spectral reflectance of the human ocular fundus. *Appl Opt* 28:1061–1077. <https://doi.org/10.1364/ao.28.001061>
40. Weiter JJ, Delori FC, Wing GL, Fitch KA (1986) Retinal pigment epithelial lipofuscin and melanin and choroidal melanin in human eyes. *Invest Ophthalmol Vis Sci* 27:145–152
41. Hayasaka S (1989) Aging changes in lipofuscin, lysosomes and melanin in the macular area of human retina and choroid. *Jpn J Ophthalmol* 33:36–42
42. Harbour JW, Brantley MA Jr, Hollingsworth H, Gordon M (2004) Association between choroidal pigmentation and posterior uveal melanoma in a white population. *Br J Ophthalmol* 88:39–43. <https://doi.org/10.1136/bjo.88.1.39>
43. Hu DN (2005) Photobiology of ocular melanocytes and melanoma. *Photochem Photobiol* 81:506–509. <https://doi.org/10.1562/2004-08-24-ir-289>
44. Wakamatsu K, Hu DN, McCormick SA, Ito S (2008) Characterization of melanin in human iridal and choroidal melanocytes from eyes with various colored irides. *Pigment Cell Melanoma Res* 21:97–105. <https://doi.org/10.1111/j.1755-148X.2007.00415.x>
45. Ung C, Lains I, Silverman RF, Woods R, Lane AM, Papakostas TD, Husain D, Miller JW, Gragoudas ES, Kim IK, Miller JB (2019) Evaluation of choroidal lesions with swept-source optical coherence tomography. *Br J Ophthalmol* 103:88–93. <https://doi.org/10.1136/bjophthalmol-2017-311586>
46. Yiu G, Vuong VS, Oltjen S, Cunefare D, Farsiu S, Garzel L, Roberts J, Thomasy SM (2016) Effect of uveal melanocytes on choroidal morphology in rhesus macaques and humans on enhanced-depth imaging optical coherence tomography. *Invest*

Ophthalmol Vis Sci 57:5764–5771. <https://doi.org/10.1167/iovs.16-20070>

47. Schraermeyer U, Addicks K, Kociok N, Esser P, Heimann K (1998) Capillaries are present in Bruch's membrane at the ora serrata in the human eye. Invest Ophthalmol Vis Sci 39:1076–1084

Publisher's note Springer Nature remains neutral with regard to jurisdictional claims in published maps and institutional affiliations.